DYNAMIC MODELLING APPROACH OF A THERMAL COMPRESSOR AND VALIDATION BASED ON EXPERIMENTAL TESTS

Ali Salame[a,b,c], Vincent Lemort[b], Pascal Dufour[c], Madiha Nadri[c], Rabah Ibsaine[a]

[a]Boostheat Company, 41-47 Bd Marcel Sembat, 69200 Vénissieux, France

[b]Energy Systems Research Unit (B49), University of Liège, Sart-Tilman, Liège 4000, Belgium

[c] Univ Lyon, Université Claude Bernard Lyon 1, CNRS, LAGEPP UMR 5007, 43 boulevard du 11 novembre 1918, F-69100, VILLEURBANNE, France

Contact Email: alisalami0980@gmail.com

ABSTRACT

A thermal compressor uses thermal energy to increase the pressure of the working gas, while maintaining a temperature difference as an essential factor for its effective functioning. The design of the thermal compressor is similar to a gamma type Stirling engine but it replaces the power piston with input and outlet valves. It also shares some technical features of a Stirling engine such as heating source flexibility, low operating noise, and potential for broad applicability in today's thermodynamic cycles. This paper first introduces the tested thermal compressor. The behavior of the instantaneous state of the fluid inside the thermal compressor is mimicked by a detailed dynamic modelling approach. A finite volume method is used to spatially discretize the system into several control volumes (CVs), and energy, mass and momentum balance equations are expressed for each control volume. This approach results in several ordinary differential equations (ODEs) that are solved and simulated in a python written script. The model is then validated with experimental data collected from a thermal compressor implemented in a real heat pump test bench.

1 INTRODUCTION

It took us four industrial revolutions and almost 250 years to realize that environmental impact is an important factor that we should prioritize in our scientific studies. Heating, being a major contributor to the total energy consumption, is an important field to navigate in order to reduce energy consumption and greenhouse gas emissions.

Heat-driven heat pump systems, which combine heating methods (like combustion) with heat pump technology, are gaining more attention today, as they offer a higher efficiency usage of fuel compared to boilers. Some innovative configurations include non-integrated systems such as a Stirling heat pump, where a Stirling engine is coupled to a compressor inside a heat pump cycle, or integrated ones like gas absorption heat pumps in Dávila et al. (2023) and Vuilleumier machines. Another integrated heat-driven heat pump systems application involves the replacement of a conventional compressor with a thermal compressor in a heat pump cycle.

The concept of a thermal compressor was first mentioned in Bush (1939) patent, and it received a wide scientific attention for several years after. Its design is usually like a gamma type Stirling engine but with the power piston replaced by two valves or an orifice. So, the kinematic mechanism coupling the displacer to the power piston is dispensed, and a motor is used to drive the displacer instead. This mechanism ensures the transportation of fluid between a heat source and a heat sink. Its technical features involve functionality under various heating sources, like biomass, fuel, and waste heat, as well as diverse applicability, like in artificial hearts by Martini (1969), pulse tube refrigerators in Dai et al. (2002) and heat pump application. A thermal compressor used in pulse-tube coolers usually require thermoacoustic power analysis, that is commonly done by connecting it to an RC load through one path as seen by Lin et al. (2013), Wang et al. (2018), and Wang et al. (2019). Wheras the ones used in

artificial hearts or Heat pump applications use two separate inlet and outlet valves, as seen in Kornhauser (1996), Edwards and Peterson (2007), and Ibsaine et al. (2016). To distinguish between the two, we use the terms “type 1” and “type 2” for the former and the latter respectively.
Due to its shared characteristics with a Stirling engine, similar modelling approaches have been utilized to model a thermal compressor. Inspired by Urieli and Berchowitz (1984), Kornhauser (1996) proposed an idealized modelling approach for a type 2 thermal compressor, providing some future insights of possible application based on some theoretical performances analyses. Edwards and Peterson (2007) extended this work by adding non-idealities. For replacing a traditional compressor in a heat pump cycle, Ibsaine at al. (2016) introduced a type 2 thermal compressor, accompanied with a 2nd order modelling approach, validated with real experimental data. Thomas and Barth (2022) investigated the effects of controlling the displacer, based on a derived dynamic model. Most of these models are 2nd order models, so they are based on energy and mass balances equations.
For a type 1 compressor, Pan et al. (2017) derived a 3rd order model by including a momentum equation. A similar approach was applied on a Stirling engine by Qui et al. (2021) and Wang et al. (2016). They validated their 3rd order model with real data showing a better prediction of the transient characteristics, as well as a better estimation of the temperature and pressure gradients inside each point in space. Moreover, Wang et al. (2018), and Wang et al. (2019) provided a detailed energy analysis for a type 1 thermal compressor.
To the best of the author's knowledge, the adoption of a 3rd order approach for type 2 thermal compressors remains unexplored within existing literature. The present work aims to fill this gap by introducing and applying a 3rd model to the design and analysis of type 2 thermal compressor, specifically introduced by Ibsaine et al. (2016). The refrigerant used is CO2, which is more environmentally friendly, as it has lower Global Warming Potential and zero Ozone Depletion Potential compared to other used refrigerants. The first section provides a description of the investigated thermal compressor, with its main components, functionality and working principle. In the third section, our system is spatially discretized, and momentum, mass, and energy balances equations are derived in the form of ODEs. The main expressions involved in the model are expanded, the flow through the valves is modeled, and the solving method is provided. Section four shares the experimental setup that allowed the collection of the data, which was further used to validate the model in the last section.

2 THERMAL COMPRESSOR DESCRIPTION

2.1 Components

A thermal compressor mainly consists of a cylinder with two varying volumes chambers and of constant volume heat exchangers that connect them. As shown in Figure 1, the cylinder is divided into two parts, compression (C) and expansion (E) spaces, separated by a displacer (D). The heat exchangers consist of a cooler (K) where the heat is rejected to the surrounding water jacket. A heater (H) that receives the heat. The regenerator (R) is made of several sheets of porous medium. It acts as a heat absorber when the fluid is moving from the upper hot part to the lower cold part, and a heat provider when the fluid flows from the cold to the hot part. Cooler dead volume (KR) and heater dead volume (HR) are formed between cooler and regenerator, and heater and regenerator respectively. Inlet and outlet vales (IV) and (OV) are connected to (C), to allow the passage of the flow.

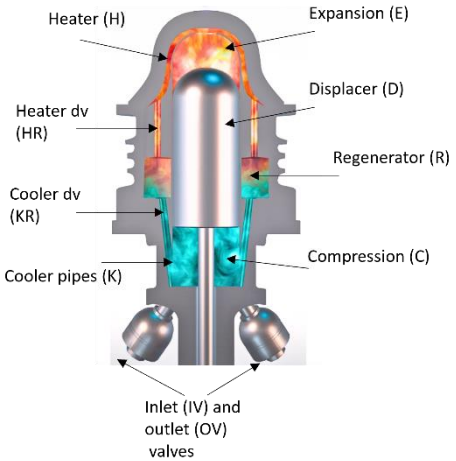

Figure 1: A vertical-cross section of the thermal compressor showings its components.

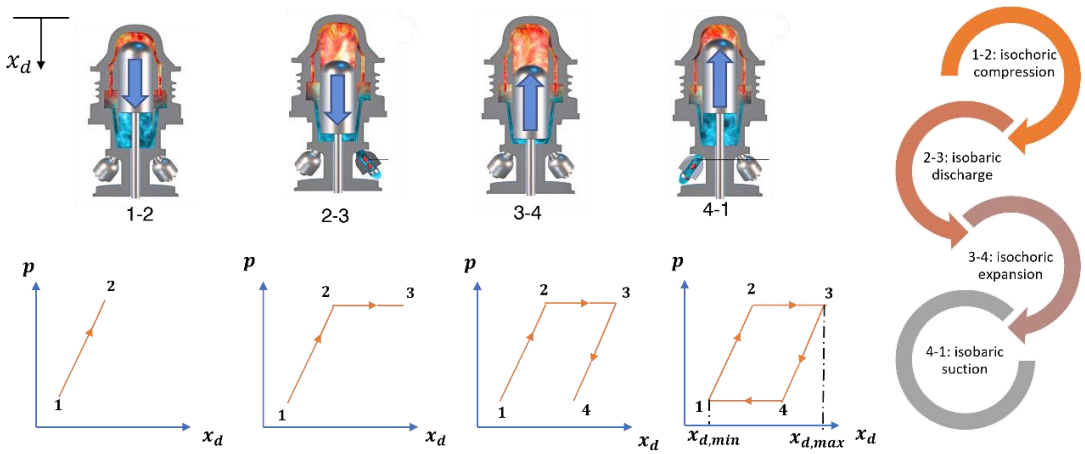

Figure 2: The variation of pressure p as a function of displacement x_d.

2.2 Thermal compression process

Unlike a traditional compressor, a thermal compressor does not rely on volume variation to create pressure waves, but rather on thermal energy. One way to describe the thermodynamic process is to show the uniform pressure variation inside the compressor as function of the displacer movement x_d. The four processes are represented in Figure 2. From phase 1 to 2, the downward movement of the displacer transports the CO2 to the upper hot part of the cylinder. Due to the high temperature, the fluid pressure gradually increases. When the pressure is high enough, the exhaust valve opens, and CO2 maintains a constant pressure from 2 to 3, assuming no pressure drop associated to the flow through the valves. At phase 3 the displacer reverses its direction of movement, and the CO2 moves again to the lower cold part, causing the gradual decrease of pressure. When the pressure is low enough (at phase 4), inlet valve opens, and CO2 returns to its initial state at 1.

2.3 Energy Conversion

An important key to understand a thermal compressor is to discuss the energy conversion processes and the thermal losses inside. The primary energy provided is heat energy resulting from an external combustion process on the top of the heater. Secondarily, electric energy is provided to the motor, which is transformed into mechanical power transmitted by the displacer to the CO2 inside. In some cases, this energy is not needed, and it can even be recovered. The useful output energy is both the increase of the CO2 enthalpy flow (corresponding to the pressure increase) and the heat that can be recovered at the low temperature source, as demonstrated in Figure 3. A detailed thermal losses analysis can be found in Wang et al. (2018) and Wang et al. (2019).

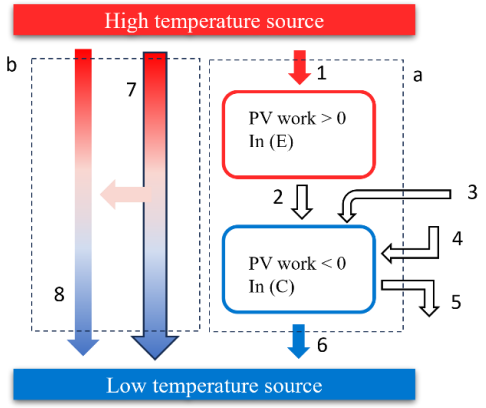

Figure 3: Energy conversion and Thermal losses.

a. Energy conversion

1- Heating power
2- Work transmitted by displacer.
3- Electric motor power
4- Input enthalpy flow.
5- Output enthalpy flow.
6- Heat rejected or Cooling power.

b. Thermal losses

7- Conduction and shuttle losses.
8- Enthalpy loss due to Cylinder-displacer gap leakages.

3 MODELLING APPROACH

The thermodynamic model derived in this section considers the following assumptions : (1) one-dimensional compressible flow, (2) kinetic and potential energy are neglected, (3) internal and external leakages are ignored, and (4) heat conduction in gas is neglected. A nomenclature is given at the paper end for symbols definition.

3.1 Governing Equations

It is necessary to consider the volume of the rod in the compression space, as it changes with time. The variation in the volume of the compression and expansion parts of the cylinder is determined by the displacement of the displacer piston. The latter is connected to a rod, which, in turn, is linked to a crank mechanism, resulting in a sinusoidal variation of volumes in (C) and (E):

$$V_c = \pi\left(r_d^2 - r_s^2\right)(l_{str} - x_d) + V_{c,min} \tag{1}$$

$$V_e = \pi\, r_d^2\, x_d + V_{e,min} \tag{2}$$

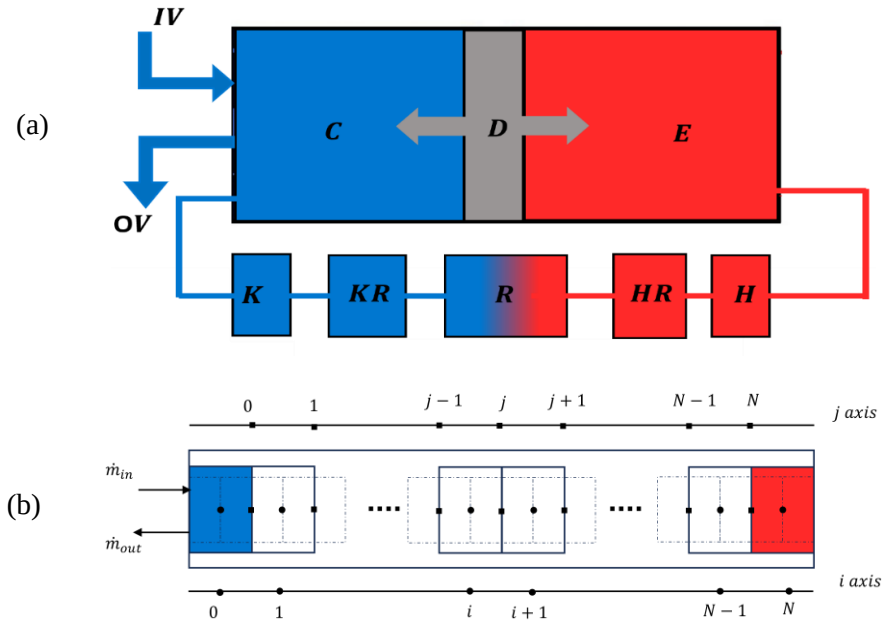

Figure 4: Schematics for (a) thermal compressor and (b) its discretized grids.

As seen in Figure 4, the system is spatially discretized using Finite Volume Method into several CVs with a corresponding $i-axis$, where each CV between adjacent solid lines represents uniform pressure, temperature, and density. The velocity and mass flow rate are considered uniform between adjacent dashed lines, corresponding to $j-axis$. This results in N+1 connected ordinary differential equations (ODEs), where the 0^{th} and the N^{th} represent the compression and expansion CVs respectively. The positive flow refers to the flow from compression to expansion chambers. The derivative of a variable x(t) is represented by $Dx = \left(\frac{\partial x}{\partial t}\right)$ when it is to be integrated, and $\dot{x}$ when it algebraically represented at each instant. Both have the same unit but serves different objectives. From a thermodynamics standpoint, Dx indicates time derivative of a point function (a thermodynamic property) while $\dot{x}$ indicates a time derivate of a path function.
Applying the mass balance on each CV results in the density variation:

$$D\rho_i = 1/V_i.\left(\dot{m}_i - \rho_i \dot{V}_i\right) \tag{3}$$

From the energy balance equation, the temperature variation is represented as

$$DT_i = 1/(m.c_v)_i.[\dot{Q}_i - T_i\left(\frac{\partial p}{\partial T}\right)_{\rho,i}\left(\dot{V}_i - \frac{1}{\rho_i}\dot{m}_i\right) - h_i\dot{m}_i + \dot{m}_{f,j-1}.h_{f,j-1} \; - \; \dot{m}_{f,j}.h_{f,j}] \quad (4)$$

$\left(\frac{\partial p}{\partial T}\right)_\rho$ being the partial derivative of p with respect to T while keeping ρ constant. The momentum balance is applied on the interfaces of the CVs to get the velocity variation equation:

$$Dv_{f,j} = 1/m_j.[A_j(p_{i-1} - p_i) + \; (\rho Av|v|)_{i-1} - (\rho Av|v|)_i \; - F_jA_j - (\rho Av|v|)_{f,j}] \quad (5)$$

The temperature variation of the walls of the heat exchangers directly in contact with the CO2 is derived from the energy balance equation as:

$$DT_{s,i} = 1/(m.c)_{s,i}.[-\dot{Q}_i + \left(-k_sA_s\frac{\partial T_s}{\partial x}\right)_{f,j-1} - \left(-k_sA_s\frac{\partial T_s}{\partial x}\right)_{f,j}] \quad (6)$$

$\dot{m}_{f,j} = (\rho vA)_{f,j}$, decides the direction of the flow between the CVs, so $h_{f,j} = h_i$ when $\dot{m}_{f,j} > 0$, and $h_{f,j} = h_{i+1}$ otherwise. $\dot{Q}_i = A_{w,i}\alpha_i(T_{s,i} - T_i)$ is the heat convection rate between the fluid and the surrounding wall. Helmholtz free energy equation of state is used to calculate the thermophysical properties of CO2 by taking temperature and density as the independent variables.

3.2 Modelling of the valves

Type 2 thermal compressor studied here is distinguished due to the utilized separated inlet and outlet valves. The used valves are of poppet type, so they are either completely opened or completely closed. The pressure difference for opening of the valves is estimated to be 0.5 bar. The flow is treated as a compressible and isentropic. The inlet and outlet mass flow rates are derived with the following equations:

$$\dot{m}_{in} = C_dA_v\rho_{in,0}\sqrt{2(h_{in} - h_{in,0})}, \qquad \text{if } p_0 < p_{in} - 0.5 \quad (7)$$

$$\dot{m}_{out} = C_dA_v\rho_{0,out}\sqrt{2(h_0 - h_{0,out})}, \qquad \text{if } p_0 > p_{out} + 0.5 \quad (8)$$

The parameters denoted with subscript $'in, 0'$ or $'0, out'$ in the equations correspond to properties associated with an isentropic flow assumption.

3.3 Energy Expressions

The energy expressions are estimated as the average of a one steady state cycle. The total power done by the displacer on (C) and (E) is calculated as:

$$\dot{W} = \omega/2\pi.\int_t^{t+T_{ss}}(p_0\dot{V}_0 + \; p_N\dot{V}_N)\,dt \quad (9)$$

Where T_{ss} is the time taken by one steady state cycle. By considering a mechanical efficiency of 85 %, the electric motor provided can be estimated as:

$$P_{motor} = \dot{W}/0.85$$

The total heat absorbed by the compressor is:

$$P_{heating} = \omega/2\pi.\int_t^{t+T_{ss}}(\sum_{heater} Q_i)\,dt \quad (10)$$

The total heat rejected by the compressor is:

$$P_{cooling} = \omega/2\pi . \int_t^{t+T_{ss}} (\sum_{cooler} Q_i)\, dt \tag{11}$$

The output power of the thermal compressor is represented by the mass flow rate multiplied by the enthalpy difference between the inlet and the outlet:

$$P_{out} = \omega/2\pi . \int_t^{t+T_{ss}} (\dot{m}_{out} h_{out} - \dot{m}_{in} h_{in})\, dt \tag{12}$$

3.4 Empirical Correlations

The friction force and the heat transfer coefficient are described as a function of frictions coefficient and Nusselt number, respectively:

$$F = \delta x . (f/d_h + K/\delta x) \rho . v . |v|/2 \tag{13}$$

$$\alpha = k . Nu/d_h \tag{14}$$

Where friction coefficient and Nusselt number are estimated based on empirical correlations depending on the state of the flow (laminar or turbulent) and the medium type. In heat exchangers and inside the cylinder:

$$f = \begin{cases} 64/Re, & Re < 2 \times 10^3 \\ 0.11(\epsilon/d_h + 68/Re)^{0.25}, & Re \geq 2 \times 10^3 \end{cases} \tag{15}$$

$$Nu = \begin{cases} 1.86(Re . Pr . d_h/\delta x)^{0.333} \left(\frac{\mu}{\mu_w}\right)^{0.14}, & Re < 2 \times 10^3 \\ 0.023 Re^{0.8} . (Pr)^n, & Re \geq 2 \times 10^3 \end{cases} \tag{16}$$

Where $n = 0.4$ for heated parts and $n = 0.3$ for cooled part. $K = K_L + \left(1 - \frac{A_1}{A_2}\right)^2$ represents the minor loss coefficient expressed as a function of bends and cross-sectional area variations.
For the porous medium regenerator:

$$f = 129/Re + 2.91 Re^{-0.103} \tag{17}$$

$$Nu = [1 + 0.99(Re . Pr)^{0.66}] \phi^{1.79} \tag{18}$$

3.5 Numerical Model Resolution

The ODEs are solved using Runge-Kutta method to the third order. The initial condition corresponds to a maximum compression volume and minimum expansion volume, as if the inlet valve has just closed. The pressure is considered uniform and equal to inlet pressure. The temperature profile of CO2 as of the solid part, are linearly distributed from a minimum at CV 1 taken equal to the cooling water temperature, and a maximum at CV N-1equivalent to the measured temperature on the tip of the heater wall. The initial density vector is calculated from the initial temperature and pressure vectors. The velocity vector is set to 0. A periodic steady state is reached when the net heat transfer rate over one cycle is close to 0 and the difference between entering and leaving mass flow rate is less than β_2.

$$\omega/2\pi . \int_t^{t+T_{ss}} \left(\sum_{reg} |Q_i|\right) dt < \beta_1 \tag{19}$$

$$\omega/2\pi . \int_t^{t+T_{ss}} (|\dot{m}_{in} - \dot{m}_{out}|)\, dt < \beta_2 \tag{20}$$

Since the thermal compressor is an open system, and due to the zero-phase difference between (C) and (E), the simulation results in a faster convergence when compared to the simulated type 1 Stirling machines.

Table 1: Parameters of the studied thermal compressor.

Component	Grid number	Parameter	Value
Compression Space	1	Clearance Volume	348.24 cm^3
Expansion Space	1	Clearance Volume	362 cm^3
Cooler	1	Type Volume	Tubes 32 cm^3
Cooler dead volume	1	Type Volume	Tubes 21 cm^3
Regenerator	12	Type Porosity Wire diameter Volume	Wired mesh screen 0.5 0.06 mm 76 cm^3
Heater dead volume (hollow cylindrical)	1	Type Volume	Annular 58 cm^3
Heater (hollow spherical)	4	Type Volume	Annular 10 cm^3

4 EXPERIMENTAL SETUP

The thermal compressor was installed in a basic heat pump cycle demonstrated in figure 5 (a). The aim of the carried experiments on this cycle was to test the general performance of a thermal compressor, without targeting the performance of the overall heat pump cycle. The cycle consists of a thermal compressor including its previously mentioned parts connected to an electric motor (M), a condenser (COND), an electronic expansion valve (EEV), and an evaporator (EVAP). The p-h diagram of CO2 in one operating point is shown in figure 5 (b). The CO2 remains in its subcritical state in the covered experiments. The heater is heated by an external combustion process, and the waste heat is recovered by a recovery heat exchanger (RHX). By removing the waste heat from the combustion power, we can get the heating power on the compressor. The cooling power is calculated from the difference of inlet and outlet water temperatures.

For validating the model, some measurements are considered as model inputs: heater temperature (on the outer surface), water temperature, inlet pressure, outlet pressure, and inlet temperature of CO2. Along with the thermal compressor parameters defined in table 1, these imposed values allow the model to predict the heating power, cooling power, electric motor power, outlet temperature and mass flow rate.

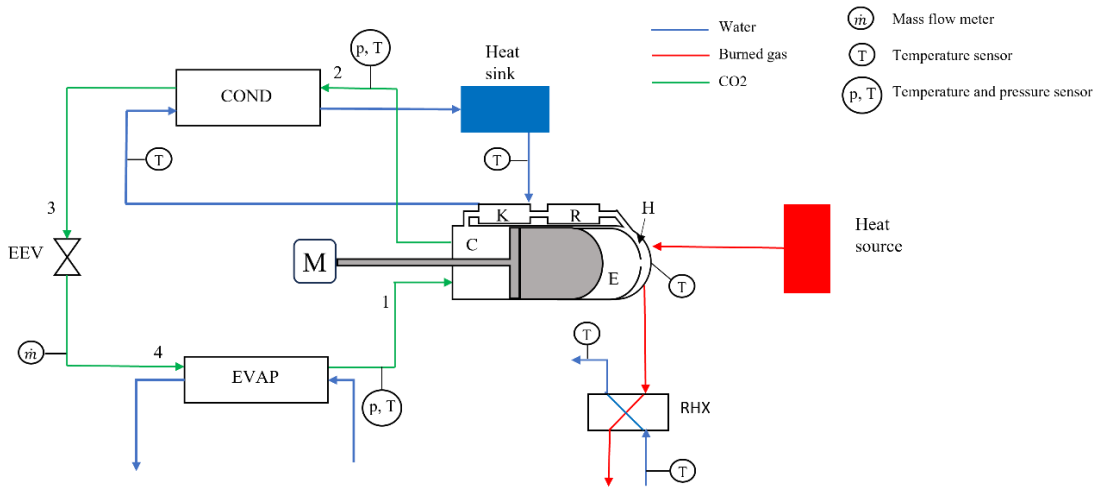

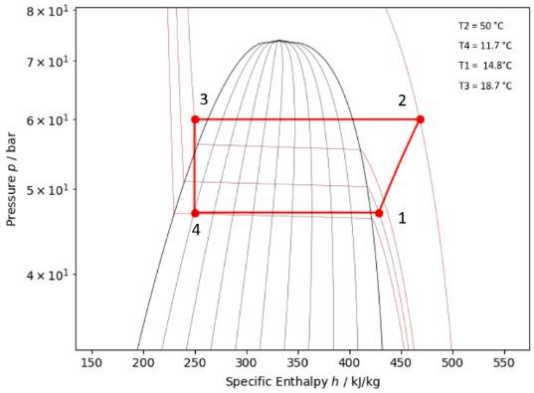

Figure 5: (a) Test Bench layout with (b) the pH diagram of CO2 in the cycle.

5 RESULTS AND DISCUSSIONS

5.1 Model Validation

The heater temperature is set at 800 °C, and the water temperature is at 20°C for all simulated (sim) and experimented (exp) points. Figure 6 illustrates how varying the pressure ratio at three different rotational speeds while the compressor is charged with CO2 at pressure 56 bar affects the compressor's performance indicators, including heating and motor power (indicating power consumption), as well as mass flow rate, CO2 outlet temperature and cooling power, highlighting the output performance. Figure 7 demonstrates these compressor's performance indicators at three different levels of charged pressure while the motor speed is fixed at 200 rpm. The uncertainties of the measured performance indicators are as follows: 5 % for powers measurements, 0.5 % for the mass flow rate, and 1 K for temperature. These uncertainties are demonstrated by the bars on the markers of the measurements in figures 6 and 7.

The figures show that when the pressure ratio increases, the heating power slightly decreases, which shows a lower heat exchange with CO2, so the pressure is not expected to increase, leading to the reduction of the mass flow rate. The increase of motor power consumption is due a higher pressure in (C) compared to (E), which would also cause the increase in the outlet temperature in (C) and thus the outlet temperature. The increase of the motor speed from 150 to 240 rpm leads to a faster flow inside the compressor, so a higher heat exchange with CO2, thus higher heating power that seems to converge after 200 rpm speed as seen in Figure 6. The mass flow rate seems to slightly change at relatively close pressure ratios, while the outlet temperature increases, leading to the increase of the output power. Figure 7 shows that the compressor admits a higher mass flow rate when the compressor is charged with higher pressure values especially at low pressure ratios. This effect converges to a minimum flow rate at a pressure ratio higher than 1.55. At higher charged pressures the heating power tends to increase, while the motor consumption power is slightly affected.

The relative of deviations of heating power prediction in Figures 6 and 7 are 8 % and 5.25 % respectively, while for the cooling power are 5.5 % and 12.47 %. On the other hand, the motor power is predicted by relative deviations of 71 % and 63.63 %. The predicted mass flow rate admits a relative of deviations of 37 % and 35.57 %, while the outlet temperature is overestimated by a deviation of 3 K, which increases much at a pressure ratio close to 1.6, specially at 200 rpm and a charged pressure value of 30 bar. The model shows an obvious underestimation of the electric or mechanical power and an overestimation of the mass flow rate, which could potentially be due to neglected mechanical losses inside the thermal compressor.

In overall, the model shows potentially good predictions for the thermal compressor performance indicators, but improvements can be made. It is recommended to extend the analysis of the valves to include their dynamics, consider the connection between the compression chamber and the motor carter that is also filled with CO2, include the displacer-cylinder gap in our analysis, and consider the friction forces caused by the seals and the displacer rings. Unfortunately, no sensors were deployed inside the compressor, so we intend to apply a three-dimensional CFD model to have some more realistic insights of the physical aspects occurring inside the compressor.

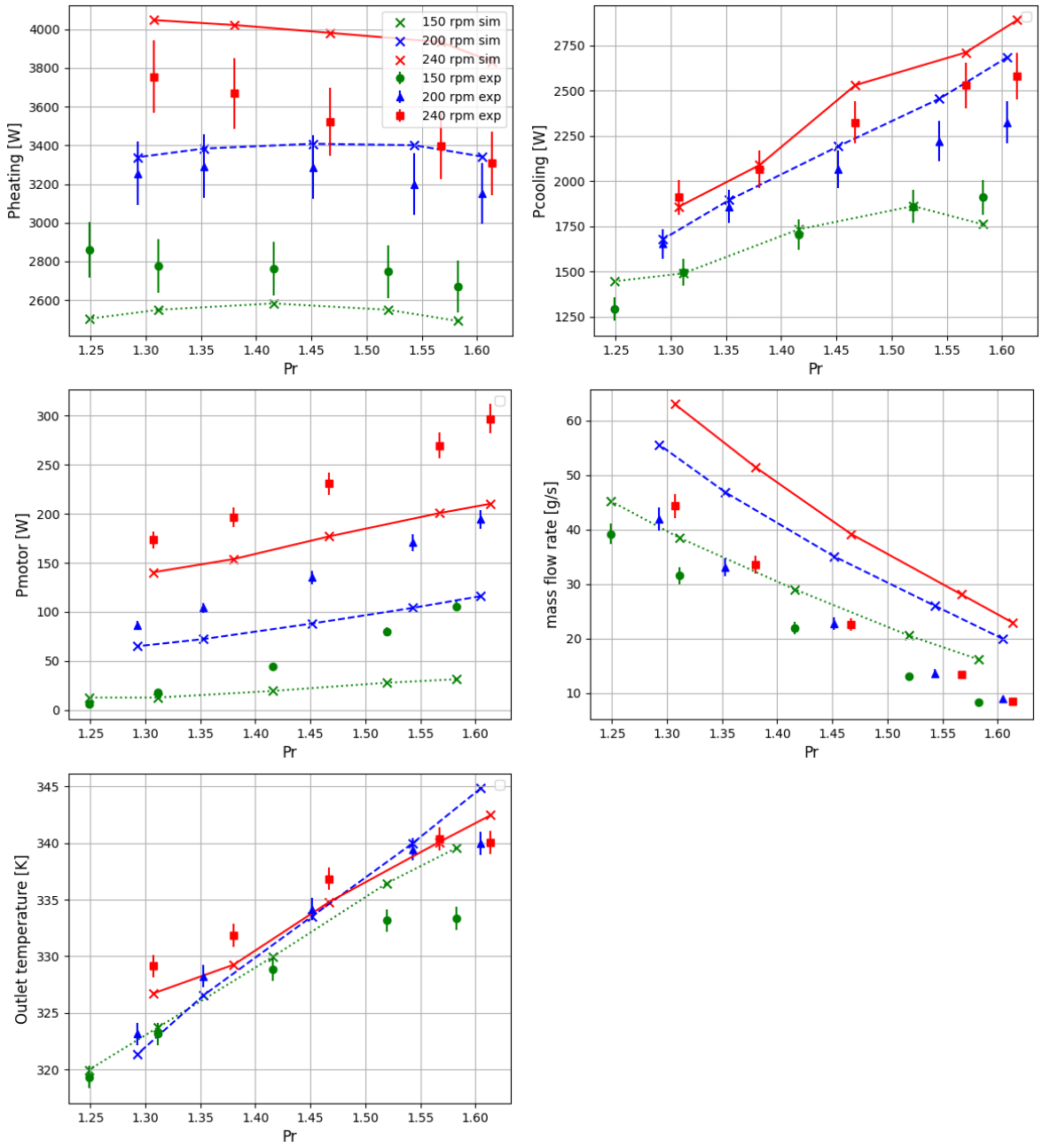

Figure 6: Compressor's performance indicators with different pressure ratios at 3 rotational speeds 150, 200 and 240 rpm.

5.2 Transient Characteristics

For a deep understanding of the working process of the thermal compressor, estimation of the transient characteristics is needed, as the process is dynamic and unsteady. The following figures are simulated at rotational speed 150 rpm, charged pressure of 56 bar and pressure ratio of 1.4. Figure 8 (a) corresponds to a p-V diagram showing the variation of pressure inside the compression and expansion spaces as a function of volumes. Figure 8 (b) depicts the instantaneous variation of CO2 temperature at the central grid of compression space, bottom of the cooler, middle of the regenerator, top of the heater, and expansion space in a cycle. Figure 8 (c) shows the variation of masses in the compression space, cooler, regenerator, heater, and expansion. The inlet and outlet mass flows variation are shown in Figure 8 (d).

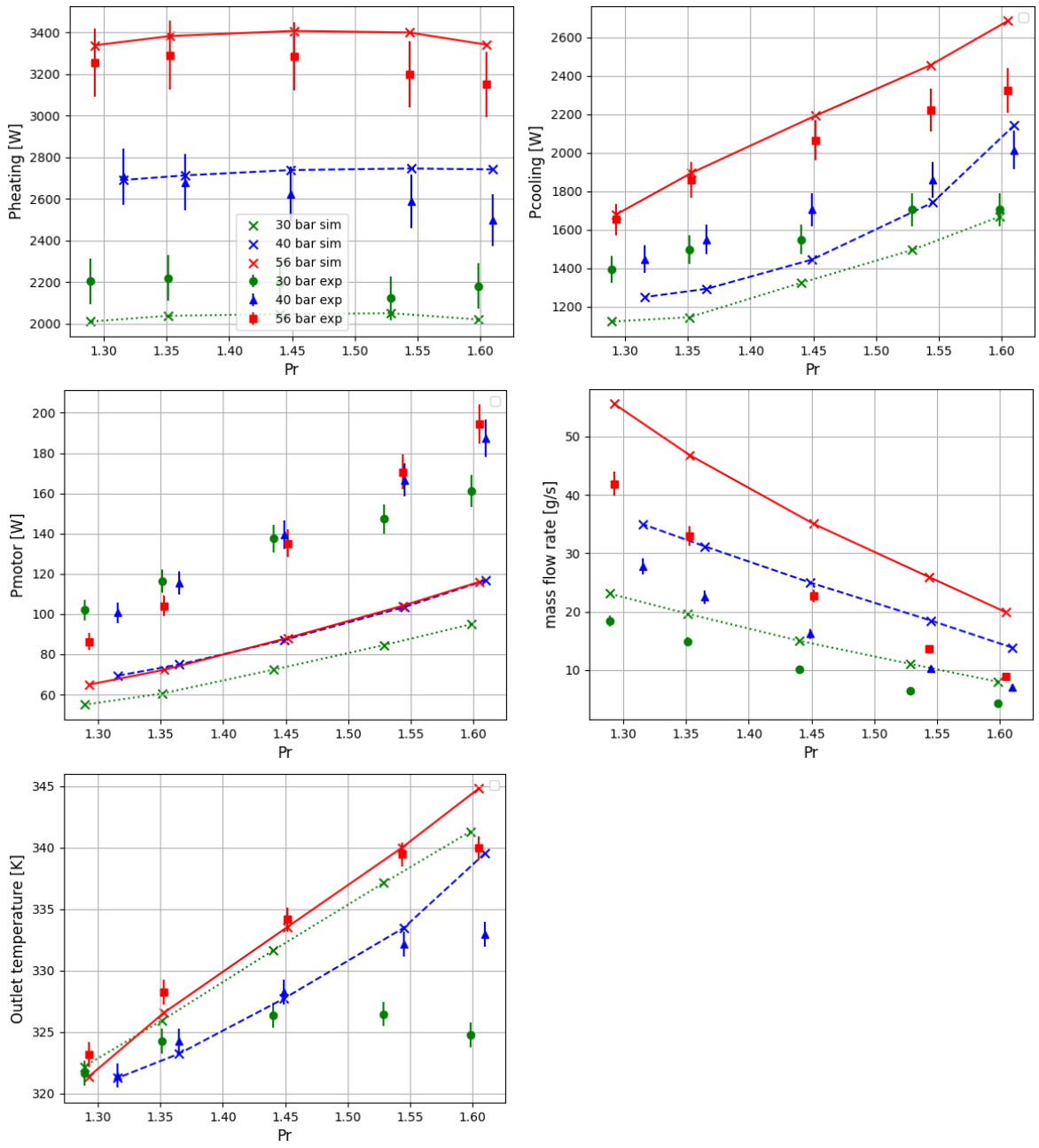

Figure 7: Compressor's performance indicators with different pressure ratios at 3 charged pressure values, 30, 40, and 56 bar.

6 CONCLUSION

A type 2 thermal compressor was introduced for heat pump applications, and a 3rd order modelling approach was proposed. The derived model was based on mass, energy, and momentum balances equations, that were applied on the CVs resulting from the discretization of the thermal compressor in space. For predicting the main performance indicators of a thermal compressor, the following average relative deviations are achieved: 6.75 % (heating power), 8.86 % (cooling power), 67.3 % (motor power), 36.3% (mass flow rate), and 3.2 K (outlet temperature). It is intended to extend the analysis of the system to include more physical effects that were neglected in this work.

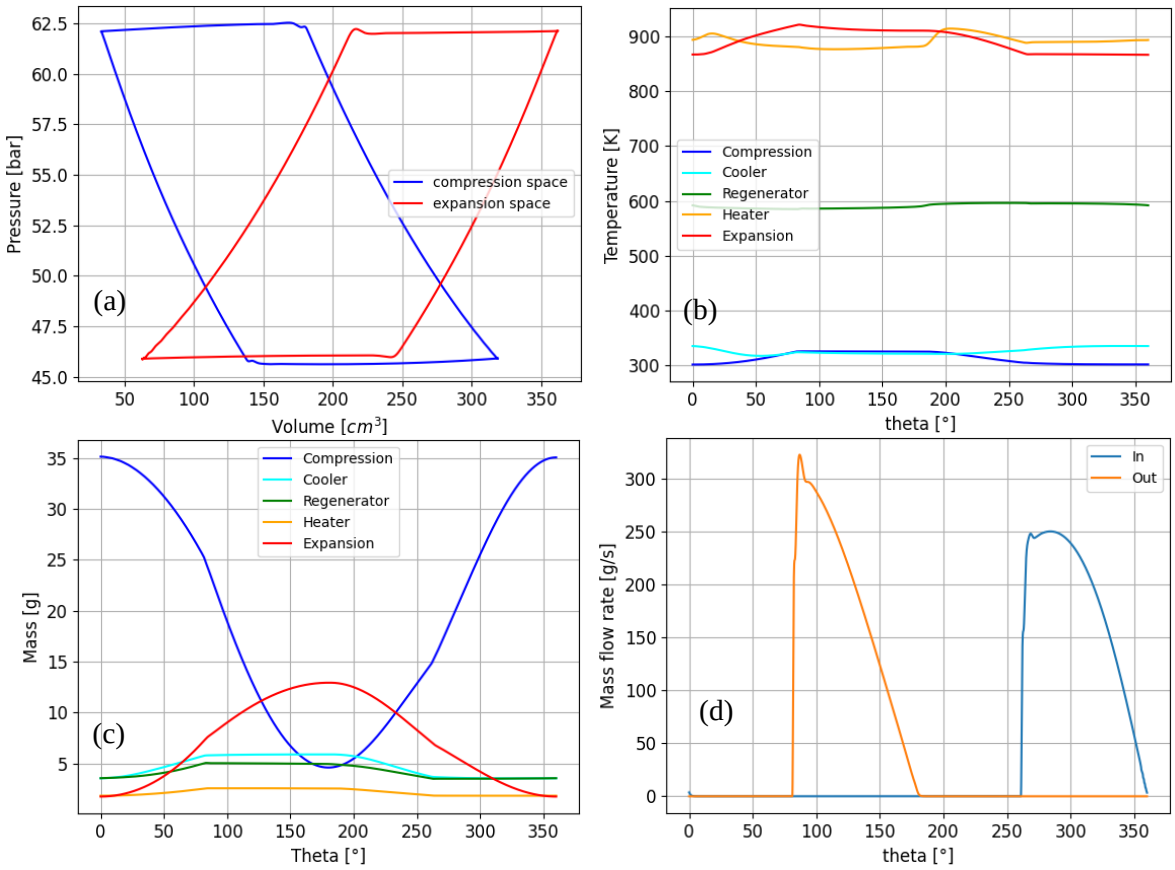

Figure 8: Model predictions of the (a) p-V diagram, (b) Temperature variations, (c) inlet and outlet flow rate, and (d) mass variations at a steady state cycle.

NOMENCLATURE

A	cross section area	(m^2)
A_w	wetted area	(m^2)
A_v	valve opening area	(m^2)
V	volume	(m^3)
c_p	isobaric specific heat	(J/kg.K)
c_v	isochoric specific heat	(J/kg.K)
c_s	specific heat of solid	(J/kg.K)
d_h	hydraulic diameter	(m)
r_d	displacer radius	(m)
r_s	shaft radius	(m)
l_{str}	stroke length	(m)
F	friction force	(N)
f	friction coefficient	(-)
K	minor loss coefficient	(-)
h	fluid enthalpy	(J/kg. K)
k	thermal conductivity	(W/m. K)
l_d	displacer length	(m)
m	mass	(kg)
$\dot{m}$	mass flow rate	(kg/s)
Nu	Nusselt number	(-)
p	pressure	(pa)
Pr	Prandtl Number	(-)

Subscripts

C	Compression
E	Expansion
K	Cooler
KR	Dead space between cooler and regenerator
R	Regenerator
HR	Dead space between heat and regenerator
H	Heater
IV	Inlet Valve
OV	Outlet Valve
s	solid
i	solid-line grid index
j	dash-line grid index
f	interface between grids
CO2	carbon dioxide

Greek symbols

ρ	density	(kg/m^3)
Φ	porosity	(-)
ϵ	roughness	(-)
μ	viscosity	(pa. s)
μ_w	viscosity of wetted area	(pa. s)
α	convection coefficient	(W/m^2. K)

$\dot{Q}$	heat transfer rate	(W)
Re	Reynolds Number	(-)
T	temperature of fluid	(K)
u	internal energy	(J/kg. K)
s	entropy	(J/kg. K)
x_d	displacement	(m)
v	velocity of fluid	(m/s)
v_d	displacer velocity	(m/s)
ω	rotational speed	(rd/s)
δx	control volume length	(m)
$\left(\frac{\partial p}{\partial T}\right)_\rho$	partial derivative	(pa/K)

Abbreviations

dv	dead volume
CV	control volume
ODE	ordinary differential equation

REFERENCES

Bell, I., 2011, Theoretical and Experimental Analysis of Liquid Flooded Compression in Scroll Compressors, Purdue University.

Bell, I.H., Wronski, J., Quoilin, S., Lemort, V., 2014, Pure and Pseudo-pure Fluid Thermophysical Property Evaluation and the Open-Source Thermophysical Property Library CoolProp, *Ind. Eng. Chem. Res.*, 53(6), p. 2498-2508.

Bush, V., 1939, "Apparatus for compressing gases," *US Patent 2,157,229*.

Dai, W., Matsubara, Y., Kobayashi, H., 2002, Experimental results on VM type pulse tube refrigerator, *Cryogenics*, Volume 42, Issues 6–7, p. 433-437.

Dávila, C., Vega, J., Lemort, V., 2023, Experimental investigation, modeling and in-situ monitoring of a gas-driven absorption heat pump in Belgium, *Cleaner Energy Systems*, Volume 6, 100087, ISSN 2772-7831.

Edwards, M.J., Peterson, R.B., 2007, Reciprocating thermocompressor performance with non-ideal component characteristics, *J. Power Energy*, 221(4), p. 459-472.

Ibsaine, R., Joffroy, J.M., Stouffs, P., 2016, Modelling of a new thermal compressor for supercritical CO2 heat pump, *Energy*, Volume 117, Part 2, p. 530-539.

Kornhauser, A.A., 1996, Analysis of an idealized stirling thermocompressor, Proc. Intersociety Energy Conversion Engineering Conference, p. 1331-1336.

Lin, W.Y., Wu, X.H., Yang, J.L., Yang, L.W., 2013, Experimental study and numerical analysis of thermocompressors with annular regenerators, *Int. J. Refrigeration*, 36(4), p. 1376-1387.

Martini, W.R., 1969, The Thermocompresor and its Application to Artificial Heart Power, Proc. 4th Intersociety Energy Conversion Engineering Conference, Washington, DC, USA, p. 107–114.

Pan, C., Wang, J., Zhang, T., Wang, J., Zhou, Y., 2017, Numerical investigation on the thermoacoustics characteristics of thermal compressor for the pulsetube cryocooler, *Applied Thermal Engineering*, 123, p. 234-242.

Qiu, H., Wang, K., Yu, P., Ni, M., Xiao, G., 2021, A third-order numerical model and transient characterization of a β-type Stirling engine, *Energy*, 222, 119973.

Thomas, S., Barth, E.J., 2022, Active Stirling Thermocompressor: Modelling and effects of controlled displacer motion profile on work output, *Applied. Energy*, 327, 120084.

Urieli, I., Berchowitz, D.M., 1984, Stirling cycle engine analysis, Adam Hilger Ltd, Bristol, UK, 646p.

Wang, J., Pan, C., Luo, K., Chen, L., Wang, J., Zhou, Y., 2018, Thermal analysis of Stirling thermocompressor and its prospect to drive refrigerator by using natural working fluid, *Energy Conversion and Management*, 177, p. 280-291.

Wang, J., Xi, X., Luo, K., Chen, L., Wang, J., Zhou, Y., 2019, Energy and exergy equilibrium analysis of Stirling-type thermal compressor (STC)—The core part in thermal-driven Vuilleumier machines, *Energy Conversion and Management*, Volume 199, 111961.

Wang, K., Dubey, S., Choo, F.H., Duan, F., 2016, A transient one-dimensional numerical model for kinetic Stirling engine, *Applied Energy*, 183, p. 775-790.

ACKNOWLEDGEMENT

The French ministry of higher education and research is acknowledged for the financial support of this CIFRE PhD thesis 2022-0549.